Acta Mech 228, 1525–1539 (2017)
DOI 10.1007/s00707-016-1774-3

ORIGINAL PAPER

Muhammad Ridwan Murshed · Shivakumar I. Ranganathan

Scaling laws in elastic polycrystals with individual grains belonging to any crystal class

Received: 1 September 2016 / Revised: 26 October 2016 / Published online: 11 January 2017

Abstract In this paper, we develop unifying scaling laws describing the response of elastic polycrystals at finite mesoscales. These polycrystals are made up of individual grains belonging to any crystal class (from cubic to triclinic) and are generated by Voronoi tessellations with varying grain sizes. Rigorous scale-dependent bounds are then obtained by setting up and solving Dirichlet and Neumann boundary value problems consistent with the Hill–Mandel homogenization condition. The results generated are benchmarked with existing numerical results in special cases and the effect of grain shape on the scaling behavior is investigated. The convergence to the effective elastic properties with increasing number of grains is established by analyzing 5180 boundary value problems. This leads to the notion of an elastic scaling function which takes a power law form in terms of the universal anisotropy index and the mesoscale. Based on the scaling function, a material scaling diagram is constructed using which the convergence to the effective properties can be analyzed for any elastic microstructure.

1 Introduction

Composite materials are widely used nowadays due to the dire need for novel materials with unique properties. With the advent of additive manufacturing, composites can be designed with superior structural integrity (enhanced fracture toughness [1]) and 3D printed with controlled variation of material properties [2,3]. Such properties are dependent upon the structure of the composite (proportions of each component, shape of the particles and arrangement of the particles) and the corresponding property of each individual component in a composite (electrical, thermal and mechanical property). Thus, the structure–property relationship is a fundamental aspect in the design of composite materials, which comprises of polycrystalline aggregates. These polycrystals are a collection of single crystals (grains) that have arbitrary orientations. The properties of polycrystalline aggregates depend upon the length scale and the single crystal orientation. By randomly assigning each crystal orientation in a polycrystal, one can obtain the effective isotropic response. In the context of elasticity, the effective property (shear and bulk moduli) can be estimated corresponding to a representative volume element (RVE).

However, determining the appropriate size of the RVE in order to accurately obtain the aggregate response is still a challenge in composite material theory. Therefore, various homogenization techniques have been developed in order to estimate the effective property. One such approach is the Mori–Tanaka method, which relates the average stress in an inclusion to the average stress in the matrix for obtaining the aggregate response

M. R. Murshed · S. I. Ranganathan (✉)
Department of Mechanical Engineering, Rowan University, 201 Mullica Hill Road, Glassboro, NJ 08028, USA
E-mail: ranganathan@rowan.edu

S. I. Ranganathan
Department of Biomedical Engineering, Rowan University, 201 Mullica Hill Road, Glassboro, NJ 08028, USA

in polycrystals (see Sevostianov and Kachanov [4]). However, the Mori–Tanakas scheme may violate the Hashin–Shtrikman bounds for multiphase composites as well as yield a non-symmetric stiffness tensor and thereby the effective response cannot be obtained. An alternative method based on Maxwell's scheme for estimating the effective property of anisotropic multiphase composites was proposed by Sevostianov [5]. In that study, the author modified Maxwell's scheme by taking into account the shape of the inclusion and illustrated that an ellipsoidal shape captured the effective response accurately. On the contrary, selecting an inappropriate shape of the inclusion will cause the stiffness and compliance tensors to lose positive definiteness, and the effective property cannot be determined.

An alternate approach to quantify the size of the RVE, free of any positive definiteness violation, is to implement the Hill–Mandel homogenization condition [6,7] and obtain rigorous bounds as solutions to scale-dependent stochastic boundary value problems (Dirichlet and Neumann). This homogenization technique has attracted a great deal of interest over the past few decades within the context of elasticity [8–12], thermal conductivity [13–16], electrical conductivity [17], thermoelasticity [18–20], flow in porous media [21–23], fracture and damage phenomena in random microstructures [24] and nonlinear elastic and inelastic materials [25–28]. This framework has been employed by several other authors including Kanit et al. [29] and El Houdaigui et al. [30] for estimating the size of the RVE. In particular, Kanit et al. [29] investigated three-dimensional Voronoi mosaic-shaped linearly elastic materials in order to determine the effective properties of two-phase heterogeneous microstructures at specific length scales. In their work, the authors showed the minimum number of realizations required for a given RVE size by taking into account the following: (i) physical property of the material; (ii) material contrast; (iii) volume fraction of individual phases; (iv) relative precision for estimating the effective property. In addition, the authors observed that for a specific precision and number of realizations, one can obtain the minimal size of the RVE in order to determine the effective response. Along similar lines, El Houdaigui et al. [30] analyzed three-dimensional Voronoi mosaic as polycrystalline morphology in order to determine the number of grains (N_G) required in an RVE for estimating the effective elastic properties of copper. The authors used a variety of boundary conditions (Dirichlet and Neumann) and obtained the mean shear modulus as a function of N_G. It was seen that the minimum number of grains required is related to the evolution of the standard deviation of the effective property (shear modulus).

Several other authors have employed the framework of stochastic micromechanics in order to demonstrate the concept of a scaling function through the convergence of Dirichlet and Neumann bounds. In particular, Ranganathan and Ostoja-Starzewski [10] obtained the scale-dependent bounds on the aggregate response of elastic random polycrystals at finite length scales. Subsequently, scaling laws were established that takes into account the mesoscale along with the universal anisotropy measure of single crystals. By employing the elastic scaling function, a material scaling diagram was constructed to quantify the size of the RVE for multifarious random polycrystals. Along similar lines, Dalaq et al. [31] illustrated the scale dependence of thermal conductivities in two-phase planar random checkerboards at all length scales. In their study, the authors analyzed microstructures with 50% volume fractions with a variety of material combinations. It was observed that the scaling function depends upon the material contrast and the mesoscale. Subsequently, a material scaling diagram was generated which estimates the size of the RVE for any combination of individual phases. Similarly, Raghavan et al. [17] examined the scale-dependent electrical conductivity of two-phase random microstructures at arbitrary volume fractions and material contrasts. In particular, the authors demonstrated the convergence of the mesoscale bounds to the effective electrical properties with increasing length scales. Also, the authors derived the scaling function, which takes into account the volume fraction, phase contrast and mesoscale. It was seen that the size of the RVE can be estimated using a material scaling diagram for a range of composite microstructures. More recently, Zhang and Ostoja-Starzewski [32] analyzed the frequency-dependent scaling function for linear viscoelastic materials. In their work, the authors numerically simulated planar random checkerboard microstructures that had volume fractions of 50% at two phases (elastic and viscoelastic), varying mesoscales ($\delta = 2, 4, 8, 16$) and frequencies (0.05–50 Hz). Next, the hierarchies of mesoscale bounds on shear- and bulk-type responses were obtained, and a scaling function was developed in order to capture the scaling trend to RVE. It was observed that the scaling function is dependent upon the frequency and the mesoscale.

In summary, a significant amount of literature is present regarding the homogenization of random composites in order to determine the effective properties. However, to the best of our knowledge there is no framework to unify the scaling behavior of elastic polycrystals belonging to any crystal class. In the present work, we will establish unifying scaling laws at finite mesoscales describing the elastic response of random polycrystals. These polycrystals are generated by Voronoi tessellations with varying grain sizes (25, 400, 1000 and 5000 grains), and the materials studied are Cu, Zn, SnF_2, S, An_{96}, Zr, α Ti and Fe_2O_3. Subsequently, rigorous

bounds are obtained at finite length scales as solutions to stochastic boundary value problems (Dirichlet and Neumann) based on the Hill–Mandel homogenization condition. The generated results are benchmarked with existing numerical solutions for Cu. We also demonstrate the effect of grain shape (Voronoi tessellations and cubic-shaped geometry) on the scaling behavior of cubic crystals (Lithium). By analyzing 5180 boundary value problems, we illustrate that the scale-dependent bounds on the elastic response of polycrystals converge to the effective properties (shear and bulk moduli) with increasing number of grains. In doing so, we generalize the notion of a scaling function through the elastic scaling function, which depends upon the universal anisotropy index and the number of grains in the domain. Finally, the scaling function will be employed to develop the material scaling diagram that allows one to precisely estimate the size of the RVE.

2 Mathematical formulation

2.1 Hill–Mandel homogenization condition

In this section, we illustrate the Hill–Mandel homogenization condition that employs the energetic and mechanistic approaches for setting up constitutive equations (see Hill [6] and Mandel [7]). First, we discuss the stress and strain fields ($\boldsymbol{\sigma}$ and $\boldsymbol{\varepsilon}$) and decompose these terms into mean and fluctuating parts as follows (see Ostoja-Starzewski [24]):

$$\begin{aligned} \boldsymbol{\sigma}(\mathbf{x},\omega) &= \bar{\boldsymbol{\sigma}}(\omega) + \boldsymbol{\sigma}'(\mathbf{x},\omega), \\ \boldsymbol{\varepsilon}(\mathbf{x},\omega) &= \bar{\boldsymbol{\varepsilon}}(\omega) + \boldsymbol{\varepsilon}'(\mathbf{x},\omega), \end{aligned} \tag{2.1}$$

where $\mathbf{x}$ is the point-to-point dependence of fluctuating fields, $\omega(\in \Omega)$ refers to a particular realization in a microstructure from the sample space, Ω, and over-bar is used to represent the volume average. Equation (2.1) will be separated into the mean and zero-mean fluctuations as follows (see Ostoja-Starzewski [24]):

$$\begin{aligned} \bar{\boldsymbol{\sigma}}_\delta(\omega) &= \frac{1}{V}\int \boldsymbol{\sigma}(\mathbf{x},\omega)\mathrm{d}V, \quad \int \boldsymbol{\sigma}'(\mathbf{x},\omega)\mathrm{d}V = 0, \\ \bar{\boldsymbol{\varepsilon}}_\delta(\omega) &= \frac{1}{V}\int \boldsymbol{\varepsilon}(\mathbf{x},\omega)\mathrm{d}V, \quad \int \boldsymbol{\varepsilon}'(\mathbf{x},\omega)\mathrm{d}V = 0. \end{aligned} \tag{2.2}$$

Here, V is the volume of the microstructure and δ is the mesoscale that can be defined as (see Ranganathan and Ostoja-Starzewski [10])

$$\delta = \frac{l}{d} = (N_{\mathrm{G}})^{\frac{1}{3}}, \tag{2.3}$$

where N_{G} is the number of grains in the microstructure, d is the characteristic length scale (for example the grain size) and l is the length scale of observation (domain size). Using Eqs. (2.1) and (2.2), the volume-averaged contracted scalar product of $\boldsymbol{\sigma}$ and $\boldsymbol{\varepsilon}$ will be defined as

$$\overline{\sigma_{ij}\varepsilon_{ij}} = \frac{1}{V}\int_V \sigma_{ij}\varepsilon_{ij}\mathrm{d}V = \bar{\sigma}_{ij}\bar{\varepsilon}_{ij} + \frac{1}{V}\int_V \sigma'_{ij}\varepsilon'_{ij}\mathrm{d}V. \tag{2.4}$$

We will now illustrate the Hill–Mandel condition which follows from Eq. (2.4) as

$$\overline{\sigma_{ij}\varepsilon_{ij}} = \bar{\sigma}_{ij}\bar{\varepsilon}_{ij}. \tag{2.5}$$

The relation Eq. (2.5) holds, provided that the following condition is satisfied:

$$\frac{1}{V}\int_V \boldsymbol{\sigma}' : \boldsymbol{\varepsilon}'\mathrm{d}V = 0. \tag{2.6}$$

Now, Green–Gauss theorem will be used in Eq. (2.6) in order to obtain the following (see Ranganathan and Ostoja-Starzewski [10]):

$$\frac{1}{V}\int_V \sigma'_{ij}\varepsilon'_{ij}\mathrm{d}V = 0 \Leftrightarrow \int_{\partial B_\delta} (t_i - \overline{\sigma_{ij}}.n_j)(u_i - \overline{\varepsilon_{ij}}.x_j)\mathrm{d}S = 0 \quad \forall x \in \partial B_\delta. \tag{2.7}$$

At this stage, we show the three types of boundary conditions that are obtained using Eq. (2.7) as follows (see Ranganathan and Ostoja-Starzewski [10], Suquet [33], Hill [34]):

(i) Uniform displacement (Dirichlet)

$$u_i = \varepsilon^0_{ij} x_j \tag{2.8a}$$

(ii) Uniform traction (Neumann)

$$t_i = \sigma^0_{ij} n_j \tag{2.8b}$$

(iii) Mixed orthogonal

$$(t_i - \sigma^0_{ij} n_j)(u_i - \varepsilon^0_{ij} x_j) = 0 \tag{2.8c}$$

One can now set up stochastic boundary value problems with the above boundary conditions, and upon ensemble averaging, the mesoscale effective response can be obtained. It has to be noted that the random field, $\boldsymbol{\Theta}(\mathbf{x})$, of material parameters involved must be spatially homogeneous and ergodic. The ensemble mean is constant, and its finite-valued covariance depends only on the shift $\mathbf{h}$ from $\mathbf{x}$ to $\mathbf{x} + \mathbf{h}$ (see Ostoja-Starzewski [20])

$$\begin{gathered} \langle \boldsymbol{\Theta}(\mathbf{x}) \rangle = \mu, \\ \langle [\boldsymbol{\Theta}(\mathbf{x}) - \langle \boldsymbol{\Theta}(\mathbf{x}) \rangle][\boldsymbol{\Theta}(\mathbf{x}+\mathbf{h}) - \langle \boldsymbol{\Theta}(\mathbf{x}+\mathbf{h}) \rangle] \rangle = K_{\boldsymbol{\Theta}}(\mathbf{h}) < \infty, \end{gathered} \tag{2.9}$$

where $\boldsymbol{\Theta}(\mathbf{x})$ is a wide-sense stationary (WSS) random field, $K_{\boldsymbol{\Theta}}(\mathbf{h})$ is the covariance function, and the ensemble averages are represented by $\langle \cdot \rangle$. We also observe that the random field, $\boldsymbol{\Theta}(\mathbf{x})$, outlined above is mean-ergodic if the spatial average (denoted by the over-bar) is equal to the ensemble average (see Ostoja-Starzewski [20])

$$\frac{1}{V} \int_V \boldsymbol{\Theta}(\omega, \mathbf{x}) \mathrm{d}V = \overline{\boldsymbol{\Theta}(\omega)} = \langle \boldsymbol{\Theta}(\mathbf{x}) \rangle = \int_\Omega \boldsymbol{\Theta}(\omega, \mathbf{x}) \mathrm{d}P, \tag{2.10}$$

where P is a probability measure related to the random field, $\boldsymbol{\Theta}(\mathbf{x})$.

The methodology for homogenization is proposed in Fig. 1. The polycrystals are generated by Voronoi tessellations using the software Neper (see Quey et al. [35]), and the grain sizes (N_G = 25, 400, 1000 and 5000) that are taken into consideration are based on the work by El Houdaigui et al. [30]. Subsequently, 5180 Dirichlet and Neumann boundary value problems are solved using Eqs. (2.8a) and (2.8b), and the scale-dependent bounds are obtained on the elastic response (shear and bulk moduli) of random polycrystals. In the next section, we will postulate a specific form of the scaling function that unifies the treatment of a wide spectrum of materials across all crystal classes (from cubic to triclinic).

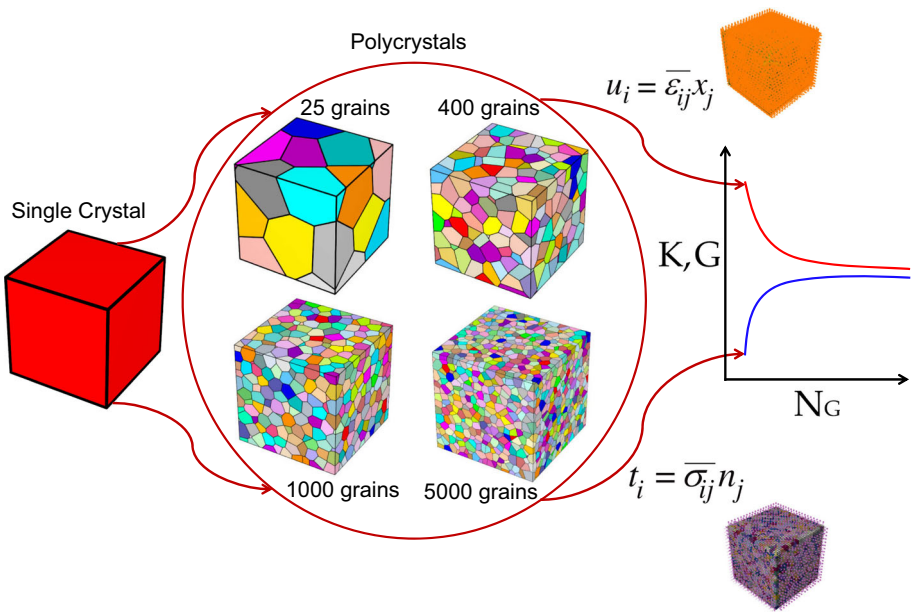

Fig. 1 Homogenization methodology

2.2 Elastic scaling function

We now discuss the scaling function for an arbitrary realization $B_\delta(\omega)$ of a random medium B_δ on a specific mesoscale δ. By using Eq. (2.8a), a stiffness tensor $\mathbf{C}_\delta^d$ can be defined as (see Ostoja-Starzewski [24])

$$\bar{\boldsymbol{\sigma}}_\delta(\omega) = \mathbf{C}_\delta^d(\omega) : \boldsymbol{\varepsilon}^0. \tag{2.11}$$

Along similar lines, Eq. (2.8b) will yield a compliance tensor $\mathbf{S}_\delta^t$ as follows (see Ostoja-Starzewski [24]):

$$\bar{\boldsymbol{\varepsilon}}_\delta(\omega) = \mathbf{S}_\delta^t(\omega) : \boldsymbol{\sigma}^0. \tag{2.12}$$

It has to be noted that for a specific mesoscale, the response of the microstructure is isotropic after ensemble averaging is carried out. Therefore, we can express the averaged stiffness and compliance tensors in terms of the bulk modulus, K as well as the shear modulus, G as follows (see Ranganathan and Ostoja-Starzewski [9]):

$$\left\langle \mathbf{C}_\delta^d \right\rangle = 2\left\langle G_\delta^d \right\rangle \mathbf{K} + 3\left\langle K_\delta^d \right\rangle \mathbf{J}, \tag{2.13a}$$

$$\left\langle \mathbf{S}_\delta^t \right\rangle = \frac{1}{2\left\langle G_\delta^t \right\rangle}\mathbf{K} + \frac{1}{3\left\langle K_\delta^t \right\rangle}\mathbf{J}, \tag{2.13b}$$

where $\mathbf{K}$ and $\mathbf{J}$ are the deviatoric and spherical components of the fourth-order identity tensor, $\mathbf{I}$. We now contract Eqs. (2.13a) and (2.13b) in order to obtain the following scalar equation (see Ranganathan and Ostoja-Starzewski [9]):

$$\left\langle \mathbf{C}_\delta^d \right\rangle : \left\langle \mathbf{S}_\delta^t \right\rangle = 5\frac{\left\langle G_\delta^d \right\rangle}{\left\langle G_\delta^t \right\rangle} + \frac{\left\langle K_\delta^d \right\rangle}{\left\langle K_\delta^t \right\rangle}. \tag{2.14}$$

By taking the limit ($\delta \to \infty$), the stiffness tensor is the exact inverse of the compliance tensor as follows (see Ranganathan and Ostoja-Starzewski [9]):

$$\lim_{\delta\to\infty} \left\langle \mathbf{C}_\delta^d \right\rangle : \left\langle \mathbf{S}_\delta^t \right\rangle = 6. \tag{2.15}$$

Rearranging Eqs. (2.14) and (2.15), we postulate the following relationship:

$$\left\langle \mathbf{C}_\delta^d \right\rangle : \left\langle \mathbf{S}_\delta^t \right\rangle = \lim_{\delta\to\infty} \left\langle \mathbf{C}_\delta^d \right\rangle : \left\langle \mathbf{S}_\delta^t \right\rangle + f(C_{ij}, A^U, \delta), \tag{2.16}$$

where $f(C_{ij}, A^U, \delta)$ is the non-dimensional function called the elastic scaling function and A^U is the universal anisotropy index that was first introduced by Ranganathan and Ostoja-Starzewski [36]. Unlike the scaling function first proposed by Ranganathan and Ostoja-Starzewski [10] that was restricted to crystals with cubic symmetry, the function in Eq. (2.16) is applicable to all crystal classes. The variable C_{ij} represents all the single-crystal elastic constants depending on the crystal class as given below:

(i) Cubic

$$C_{ij} \equiv (C_{11}, C_{12}, C_{44}) \tag{2.17a}$$

(ii) Hexagonal

$$C_{ij} \equiv (C_{11}, C_{12}, C_{13}, C_{33}, C_{44}) \tag{2.17b}$$

(iii) Tetragonal

$$C_{ij} \equiv (C_{11}, C_{12}, C_{13}, C_{33}, C_{44}, C_{66}) \tag{2.17c}$$

(iv) Trigonal

$$C_{ij} \equiv (C_{11}, C_{12}, C_{13}, C_{14}, C_{33}, C_{44}) \tag{2.17d}$$

(v) Orthorhombic

$$C_{ij} \equiv (C_{11}, C_{12}, C_{13}, C_{22}, C_{23}, C_{33}, C_{44}, C_{55}, C_{66}) \tag{2.17e}$$

(vi) Monoclinic

$$C_{ij} \equiv (C_{11}, C_{12}, C_{13}, C_{15}, C_{22}, C_{23}, C_{25}, C_{33}, C_{35}, C_{44}, C_{46}, C_{55}, C_{66}) \tag{2.17f}$$

(vii) Triclinic

$$\begin{aligned} C_{ij} \equiv (&C_{11}, C_{12}, C_{13}, C_{14}, C_{15}, C_{16}, C_{22}, C_{23}, C_{24}, C_{25}, C_{26}, \\ &C_{33}, C_{34}, C_{35}, C_{36}, C_{44}, C_{45}, C_{46}, C_{55}, C_{56}, C_{66}) \end{aligned} \tag{2.17g}$$

Substituting Eqs. (2.15) and (2.16) into Eq. (2.14) gives the functional form of the elastic scaling function as

$$f(C_{ij}, A^U, \delta) = 5\frac{\langle G_\delta^d \rangle}{\langle G_\delta^t \rangle} + \frac{\langle K_\delta^d \rangle}{\langle K_\delta^t \rangle} - 6. \tag{2.18}$$

The boundary value problems listed under Eqs. (2.8a) and (2.8b) can be solved numerically in order to obtain the right-hand side of Eq. (2.18). In the next section, we will discuss the upper and lower bounds on the elastic property (bulk and shear moduli) of materials.

2.3 Bounds on the bulk and shear moduli

The hierarchy of scale-dependent bounds on the elastic response of random microstructures will be shown by employing the spatial ergodicity, WSS properties and the variational principles of continuum elasticity as follows (see Ostoja-Starzewski [24], Kanit et al. [29], Sab [37], Huet [38])

$$\langle \mathbf{S}_1^t \rangle^{-1} \leq \cdots \leq \langle \mathbf{S}_{\delta'}^t \rangle^{-1} \leq \langle \mathbf{S}_\delta^t \rangle^{-1} \leq \cdots \leq \mathbf{C}_\infty^{\text{eff}} \cdots \leq \left\langle \mathbf{C}_\delta^d \right\rangle \leq \left\langle \mathbf{C}_{\delta'}^d \right\rangle \cdots \leq \left\langle \mathbf{C}_1^d \right\rangle \quad \forall \delta' \leq \delta. \tag{2.19}$$

We now illustrate the hierarchy of bounds on the bulk and shear moduli for isotropic stiffness tensors using Eq. (2.19) as follows (see Ranganathan and Ostoja-Starzewski [9] and Ostoja-Starzewski et al. [39]):

$$K^{\text{R}} \leq \cdots \leq \langle K_{\delta'}^t \rangle \leq \langle K_\delta^t \rangle \leq \cdots \leq K_\infty^{\text{eff}} \cdots \leq \left\langle K_\delta^d \right\rangle \leq \left\langle K_{\delta'}^d \right\rangle \cdots \leq K^{\text{V}} \quad \forall \delta' \leq \delta, \tag{2.20a}$$

$$G^{\text{R}} \leq \cdots \leq \langle G_{\delta'}^t \rangle \leq \langle G_\delta^t \rangle \leq \cdots \leq G_\infty^{\text{eff}} \cdots \leq \left\langle G_\delta^d \right\rangle \leq \left\langle G_{\delta'}^d \right\rangle \cdots \leq G^{\text{V}} \quad \forall \delta' \leq \delta, \tag{2.20b}$$

where K^{V} and K^{R} are the Voigt and Reuss estimates for the bulk modulus, respectively (see Hill [40]). Similarly, G^{V} and G^{R} are the Voigt and Reuss bounds for the shear modulus. In the subsequent section, we will illustrate the properties and bounds on the scaling function.

2.4 Properties and bounds on the elastic scaling function

The elastic scaling function $f(C_{ij}, A^U, \delta)$ that is postulated in Eq. (2.16) has the following properties:

$$f(C_{ij}, A^U, \delta = \infty) = 0, \tag{2.21}$$

where the scaling function is equal to zero when the mesoscale is infinite. Also, when the single crystals are locally isotropic ($A^U = 0$), the scaling function is equal to zero:

$$f(C_{ij}, A^U = 0, \delta) = 0. \tag{2.22}$$

We now demonstrate the bounds of the elastic scaling function as follows:

$$f(C_{ij}, A^U, \delta = \infty) \leq f(C_{ij}, A^U, \delta) \leq f(C_{ij}, A^U, \delta = 1) \quad \forall 1 \leq \delta \leq \infty. \tag{2.23}$$

Now, we use Eqs. (2.21) and (2.18) in (2.23) in order to get the following:

$$0 \leq f(C_{ij}, A^U, \delta) \leq A^U = 5\frac{G_V}{G_R} + \frac{K_V}{K_R} - 6 \quad \forall 1 \leq \delta \leq \infty. \tag{2.24}$$

It has to be noted that if C_{ij} is changed to $\alpha\, C_{ij}$ (α is a real number), the scaling function f remains the same:

$$f(\alpha\, C_{ij}, A^U, \delta) = f(C_{ij}, A^U, \delta). \tag{2.25}$$

It is therefore possible to postulate the various forms of the scaling function once the parameters of f are identified.

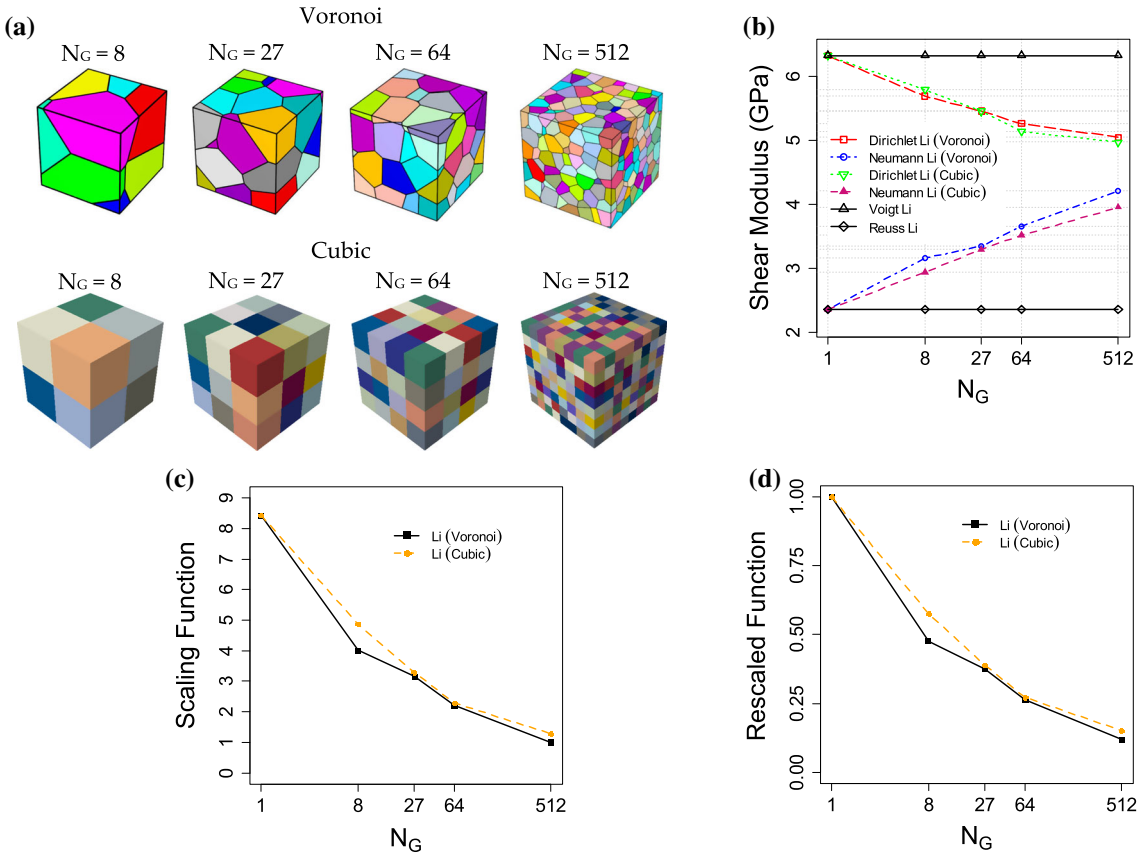

Fig. 2 Comparison of grain shapes for lithium: **a** Voronoi and cubic-shaped geometry. **b** Scale-dependent bounds for the shear modulus. **c** Scaling function. **d** Rescaled function

3 Results and discussion

We now illustrate the rigorous bounds on the elastic properties of random polycrystals at finite length scales. These polycrystals are generated numerically according to spatially ergodic and WSS properties. Also, the polycrystals are white-noise random fields as these have no spatial correlations. In the subsequent sections, we validate our numerical results for the shear modulus of Cu with the results published in the literature by El Houdaigui et al. [30]. After validating the numerical model, we study the effect of grain shape (Voronoi tessellations and cubic-shaped geometry) on the scaling function as well as the size of the RVE (see Fig. 2). Then, we will study 8 materials (see Table 1) across all crystal classes (from cubic to triclinic) and perform 5180 numerical simulations in order to illustrate the scale-dependent bounds on the aggregate elastic response. In doing so, we impose Dirichlet and Neumann boundary conditions on polycrystals with varying grain sizes (25, 400, 1000 and 5000) as follows:

(1) Dirichlet problem:
(i) For extracting shear modulus: $\varepsilon^0_{11} = \varepsilon^0_{22} = 0.05,\ \varepsilon^0_{33} = -0.1,\ \varepsilon^0_{12} = \varepsilon^0_{13} = \varepsilon^0_{23} = 0$;
(ii) For extracting bulk modulus: $\varepsilon^0_{11} = \varepsilon^0_{22} = \varepsilon^0_{33} = 0.05,\ \varepsilon^0_{12} = \varepsilon^0_{13} = \varepsilon^0_{23} = 0$;
(2) Neumann problem:
(iii) For extracting shear modulus: $\sigma^0_{11} = \sigma^0_{22} = 16$ GPa, $\sigma^0_{33} = -32$ GPa, $\sigma^0_{12} = \sigma^0_{13} = \sigma^0_{23} = 0$;
(iv) For extracting bulk modulus: $\sigma^0_{11} = \sigma^0_{22} = \sigma^0_{33} = 16$ GPa, $\sigma^0_{12} = \sigma^0_{13} = \sigma^0_{23} = 0$.

Next, we will proceed to develop a suitable form of the scaling function and construct the material scaling diagram for quantifying the size of the RVE.

Table 1 Materials analyzed across all crystal classes

Crystal class	Material	G_V (GPa)	G_R (GPa)	K_V (GPa)	K_R (GPa)	A^U
Cubic	Cu[a]	54.63	40.03	137.07	137.07	1.82
Hexagonal	Zn[b]	44.82	34.13	75.08	61.58	1.79
Monoclinic	SnF_2[c]	13.8	10.3	17.9	16.5	1.78
Orthorhombic	S[d]	7.22	6.17	20.6	17.56	1.03
Triclinic	An^{e}_{96}	42.45	35.70	88.74	84.1	0.99
Tetragonal	Zr[f]	21.7	18.4	21	19	1.00
Hexagonal	α Ti[g]	44.2	42.59	105	105	0.19
Trigonal	Fe_2O_3[h]	94.7	91.9	98.3	97.2	0.16

[a] El Houdaigui et al. [30]; [b] Berryman [42]; [c] Watt [43]; [d] Lide [44]; [e] Brown et al. [45]; [f] Watt and Peselnick [46]; [g] Ledbetter and Kim [47]; [h] Berryman [42]

Table 2 Model validation for shear modulus of Cu (Dirichlet)

No. of grains	No. of realizations	Current work	El Houdaigui et al. [30]	% difference
25	100	51.77	52.54	1.48
400	50	50.03	50.09	0.12
1000	25	49.94	49.79	0.31
5000	10	49.48	49.34	0.29

Table 3 Model validation for shear modulus of Cu (Neumann)

No. of grains	No. of realizations	Current work	El Houdaigui et al. [30]	% difference
25	100	44.90	43.4	3.47
400	50	47.15	47.31	0.34
1000	25	47.49	47.57	0.15
5000	10	48.17	48.39	0.46

3.1 Benchmark results

We discuss the benchmarking studies that were performed in order to validate the results for Cu with the ones published in the literature by El Houdaigui et al. [30]. For Dirichlet boundary value problems, computational results showed that the scale-dependent bounds converged to the effective property (shear modulus) as the percentage difference is less than 2% for all grain sizes (see Table 2). Similarly, for Neumann boundary value problems, numerical results indicated that the bounds approached the effective property as the percentage difference is less than 4% for all grains sizes (see Table 3). In the subsequent section, we will illustrate the effect of grain shape on the scaling behavior of random microstructures.

3.2 Effect of grain shape on scaling function and size of RVE

We now consider the effect of the grain shape on the scaling behavior of lithium as its universal anisotropy index is very high ($A^U = 8.4256$). In addition, we have selected the grain sizes (8, 27, 64 and 512) based on the work by Ranganathan and Ostoja-Starzewski [10] (see Fig. 2a). We now compare the scale-dependent bounds on the shear modulus for grains generated by Voronoi tessellations and cubic-shaped grains (see Fig. 2b). It can be seen that as $N_G \to \infty$ ($\delta \to \infty$), there is no significant difference in the results obtained using the geometry generated by Voronoi tessellations and the cubic-shaped geometry. This is consistent with the observations of Ranganathan and Ostoja-Starzewski [10] and Bhattacharya and Suquet [41]. In fact, we observe the scaling and rescaled functions to be almost identical except for $N_G = 8$ (see Fig. 2c, d). Therefore, we conclude that it does not matter whether one uses Voronoi or cubic-shaped geometry in order to quantify the size of the RVE. Also, if A^U is significantly large, the shape of the grains is not important for homogenizing the aggregate response. In addition, the RVE size is not affected by the grain shape when $A^U = 0$. We now proceed to demonstrate the scale-dependent bounds of all the materials analyzed across the various crystal classes.

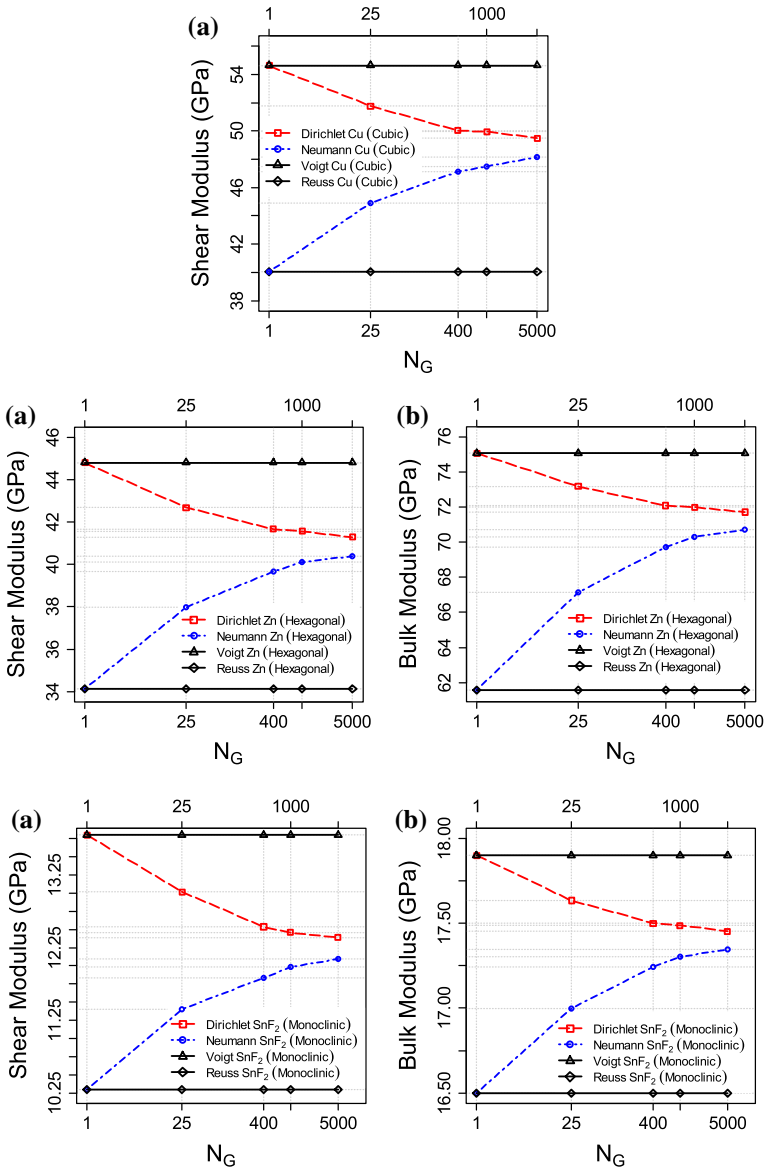

Fig. 3 Scale-dependent bounds for the elastic moduli of Cu (*top*), Zn (*center*) and SnF_2 (*bottom*): **a** shear modulus. **b** bulk modulus

3.3 Scale-dependent bounds on the effective response

We now illustrate the scale-dependent response of the microstructures, which are obtained by solving Dirichlet and Neumann boundary value problems. The upper and lower bounds for all materials studied correspond to the Voigt and Reuss estimates. The scale-dependent bounds of the shear modulus for Cu as well as the bounds for the shear and bulk moduli for Zn and SnF_2 are observed in Fig. 3. It is evident that the bounds converge to the effective property with an increase in the number of grains from 25 to 5000 (see Fig. 3). Along similar lines, the scale-dependent bounds of S, An_{96} and Zr get tighter as the number of grains increases (see Fig. 4). Similarly, the elastic response of α Ti and Fe_2O_3 indicates that the bounds approach the effective property (shear and bulk moduli) as the grain size increases (see Fig. 5).

Let us now consider the scaling behavior of all the materials studied. The universal anisotropy index, A^U, for Cu, Zn and SnF_2 is almost identical (see Table 1), and therefore, they will be analyzed together. Figure 6 shows that the scaling functions for these materials are quite close to one another, and it is reasonable to state

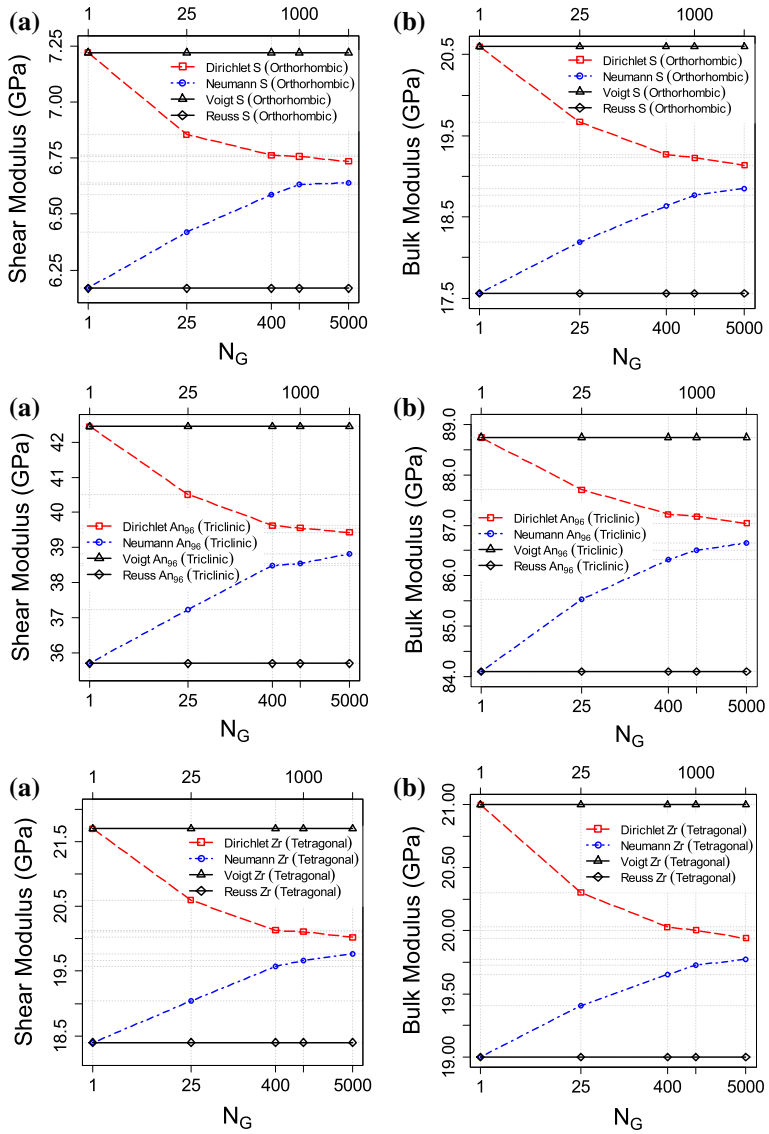

Fig. 4 Scale-dependent bounds for the elastic moduli of S (*top*), An_{96} (*center*) and Zr (*bottom*): **a** shear modulus. **b** bulk modulus

that the scaling function depends only on the A^U and the mesoscale, δ. Therefore, we rewrite Eq. (2.18) as follows:

$$f(C_{ij}, A^U, \delta) \equiv f(A^U, \delta). \tag{3.1}$$

We now discuss the scaling functions for S, An_{96} and Zr (see Fig. 6). Once again, the scaling functions for these three materials are very close to each other. A similar phenomenon is observed for α Ti and Fe_2O_3 as the scaling functions for these two materials are almost identical (see Fig. 6).

4 Constructing the scaling function

We now rewrite Eq. (2.24) in order to illustrate the functional form of the scaling function as follows:

$$0 \leq \frac{1}{A^U} f(A^U, \delta) \leq 1. \tag{4.1}$$

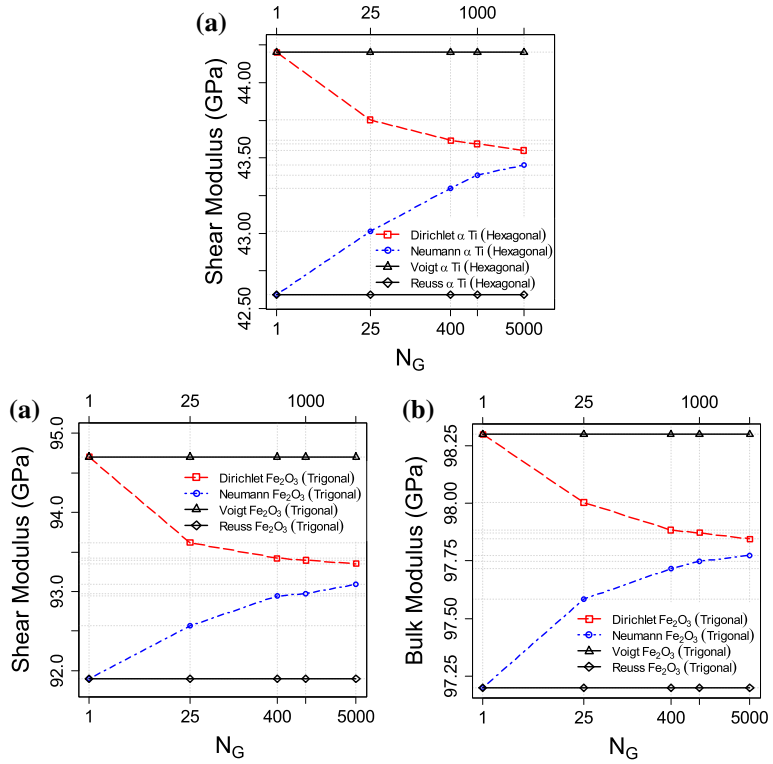

Fig. 5 Scale-dependent bounds for the elastic moduli of α Ti (*top*) and Fe_2O_3 (*bottom*): **a** shear modulus. **b** bulk modulus

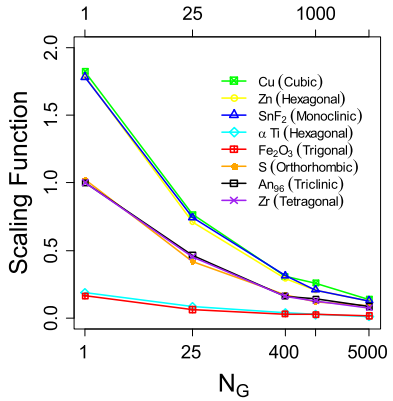

Fig. 6 Scaling function for all materials

Let us now consider the rescaled scaling function defined in Eq. (4.1). It is very interesting to observe that the rescaled function is identical for all the materials belonging to any crystal class as shown in Fig. 7. The slight scatter in the results plotted in Fig. 7 can be attributed to the finite number of realizations used to obtain the ensemble averages. Therefore, it is reasonable to state that the rescaled function, f^*, is independent of the universal anisotropy index, A^U, and is only a function of the mesoscale, δ. We now proceed to redefine the scaling function as follows:

$$f(A^U, \delta) = A^U f^*(\delta), \tag{4.2}$$

where $f^*(\delta)$ is the material independent rescaled function. We now take the mean values of $f^*(\delta)$ in Fig. (7) to construct the effective averaged rescaled function and curve fit it (see Fig. 8). Based on the effective function and its fit, $f^*(\delta)$ takes the following form:

$$f^*(\delta) = (\delta)^{-0.89}. \tag{4.3}$$

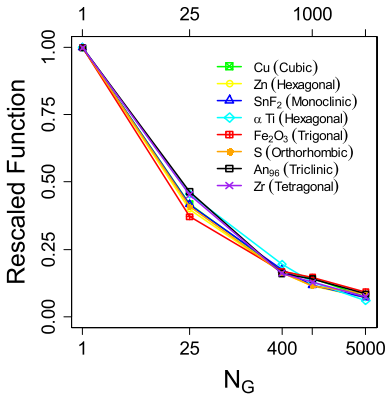

Fig. 7 Rescaled scaling function for all materials

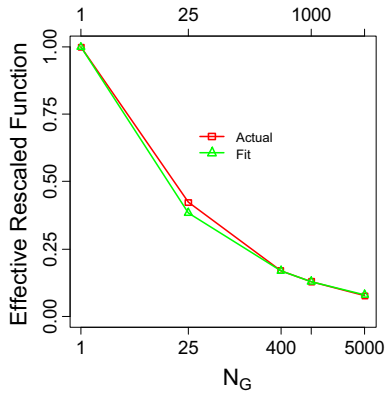

Fig. 8 Effective rescaled scaling function and fit for all materials

At this stage, it is convenient to illustrate the scaling function using Eqs. (4.2) and (4.3) as follows:

$$f(A^U, \delta) = A^U(\delta)^{-0.89}, \quad \delta = (N_G)^{\frac{1}{3}}. \tag{4.4}$$

This form of the scaling function takes into account all the properties defined in Sect. 2.4. We now employ Eq. (4.4) to reconstruct the scaling function for all the materials as shown in Fig. 9. It is clear from this plot that this formulation captures the scaling function accurately and unifies the treatment of a wide spectrum of materials across all crystal classes (from cubic to triclinic).

5 Material scaling diagram

We now discuss the contours of the scaling function in the (A^U, N_G) space based on Eq. (4.4) (see Fig. 10). It can be seen that, as the scaling function decreases, the curves shift toward the higher number of grains and vice versa. It has to be noted that the value of the scaling function determines the appropriate size of the RVE. Theoretically, when the number of grains is infinite, the scaling function becomes zero or when $A^U = 0$ (crystal is locally isotropic). For practical purposes, one can choose a finite value of the scaling function in order to determine the number of grains required for homogenization. We illustrate this concept by choosing a specific value of the scaling function ($f = 0.2$) and construct Fig. 11 based on this value for a variety of elastic random polycrystals across all crystal classes (from cubic to triclinic). For a material with low anisotropy (Fe_2O_3), the RVE is approached at $N_G = 1$ ($\delta = 1$). Finally, for a material with high anisotropy (Cu), the number of grains required for homogenization is $N_G = 1678$ ($\delta \cong 12$).

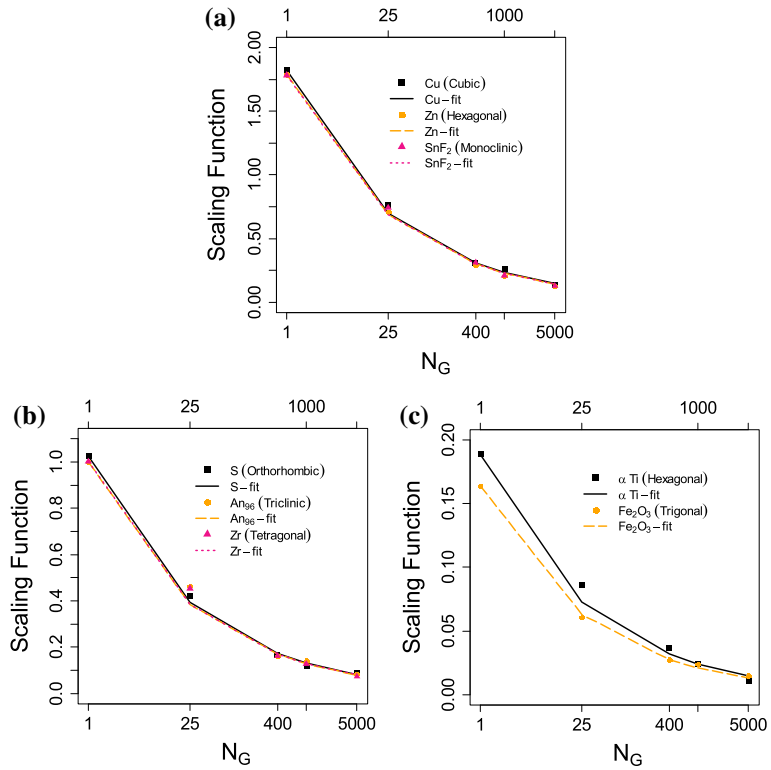

Fig. 9 Scaling functions and fit using Eq. (4.4) for all materials **a** Cu, Zn, SnF_2. **b** S, An_{96}, Zr. **c** α Ti, Fe_2O_3

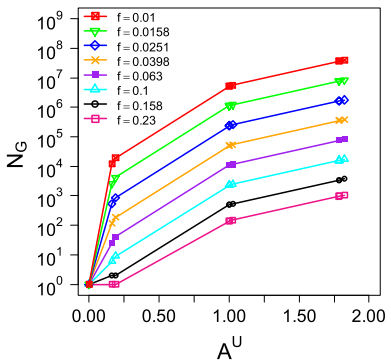

Fig. 10 Contours of the scaling function for $0.01 \leq f \leq 0.23$

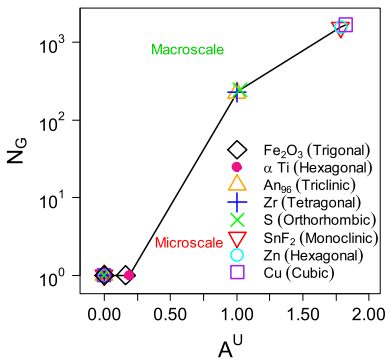

Fig. 11 Material scaling diagram at $f = 0.2$

6 Conclusion

In this paper, we have demonstrated the methodology to obtain scale-dependent bounds on the elastic response of polycrystals by solving stochastic boundary value problems (Dirichlet and Neumann) consistent with the Hill–Mandel homogenization condition. In doing so, we established a framework to unify the treatment of a variety of elastic random polycrystals across all crystal classes (from cubic to triclinic) in terms of the elastic scaling function. This specific form of the scaling function takes into account the universal anisotropy index (A^U) and the number of grains in the domain. In addition, we have shown some characteristics of the scaling function such as that the scaling function is zero at infinite grain sizes or when the crystals are locally isotropic ($A^U = 0$). Subsequently, a material scaling diagram is constructed that allows one to estimate the number of grains required to homogenize the aggregate response in order to accurately determine the effective property. In the current work, we have employed only two of the three boundary conditions that stem from the Hill–Mandel condition. In the future, one can analyze the effect of the third (mixed orthogonal) boundary condition on the elastic scaling function. To the best of our knowledge, this is the first attempt to unify the scaling behavior for elastic polycrystals belonging to any crystal class.

Acknowledgements S.I.R. was supported by the start-up grant from Rowan University.

References

1. Murshed, M.R., Ranganathan, S.I., Abed, F.H.: Design maps for fracture resistant functionally graded materials. Eur. J. Mech. A Solids **58**, 31–41 (2016)
2. Schumacher, C., Bickel, B., Rys, J., Marschner, S., Daraio, C., Gross, M.: Microstructures to control elasticity in 3D printing. ACM Trans. Graph. **34**(4), 136 (2015)
3. Oxman, N.: Variable property rapid prototyping: inspired by nature, where form is characterized by heterogeneous compositions, the paper presents a novel approach to layered manufacturing entitled variable property rapid prototyping. Virtual Phys. Prototyp. **6**(1), 3–31 (2011)
4. Sevostianov, I., Kachanov, M.: On some controversial issues in effective field approaches to the problem of the overall elastic properties. Mech. Mater. **69**(1), 93–105 (2014)
5. Sevostianov, I.: On the shape of effective inclusion in the Maxwell homogenization scheme for anisotropic elastic composites. Mech. Mater. **75**, 45–59 (2014)
6. Hill, R.: Elastic properties of reinforced solids: some theoretical principles. J. Mech. Phys. Solids **11**(5), 357–372 (1963)
7. Mandel, J.: Contribution théorique à l'étude de l'écrouissage et des lois de l'écoulement plastique. In: Görtler, H. (ed.) Applied Mechanics, pp. 502–509. Springer, Berlin (1966)
8. Raghavan, B.V., Ranganathan, S.I.: Bounds and scaling laws at finite scales in planar elasticity. Acta Mech. **225**(11), 3007–3022 (2014)
9. Ranganathan, S.I., Ostoja-Starzewski, M.: Towards scaling laws in random polycrystals. Int. J. Eng. Sci. **47**(11), 1322–1330 (2009)
10. Ranganathan, S.I., Ostoja-Starzewski, M.: Scaling function, anisotropy and the size of RVE in elastic random polycrystals. J. Mech. Phys. Solids **56**(9), 2773–2791 (2008)
11. Khisaeva, Z., Ostoja-Starzewski, M.: On the size of RVE in finite elasticity of random composites. J. Elast. **85**(2), 153–173 (2006)
12. Jiang, M., Alzebdeh, K., Jasiuk, I., Ostoja-Starzewski, M.: Scale and boundary conditions effects in elastic properties of random composites. Acta Mech. **148**(1–4), 63–78 (2001)
13. Dalaq, A.S., Ranganathan, S.I.: Invariants of mesoscale thermal conductivity and resistivity tensors in random checkerboards. Eng. Comput. **32**(6), 1601–1618 (2015)
14. Kale, S., Saharan, A., Koric, S., Ostoja-Starzewski, M.: Scaling and bounds in thermal conductivity of planar gaussian correlated microstructures. J. Appl. Phys. **117**(10), 104301 (2015)
15. Ranganathan, S.I., Ostoja-Starzewski, M.: Mesoscale conductivity and scaling function in aggregates of cubic, trigonal, hexagonal, and tetragonal crystals. Phys. Rev. B **77**(21), 214308 (2008)
16. Ostoja-Starzewski, M., Schulte, J.: Bounding of effective thermal conductivities of multiscale materials by essential and natural boundary conditions. Phys. Rev. B **54**(1), 278 (1996)
17. Raghavan, B.V., Ranganathan, S.I., Ostoja-Starzewski, M.: Electrical properties of random checkerboards at finite scales. AIP Adv. **5**(1), 017131 (2015)
18. Du, X., Ostoja-Starzewski, M.: On the scaling from statistical to representative volume element in thermoelasticity of random materials. Netw. Heterog. Media **1**(2), 259 (2006)
19. Khisaeva, Z., Ostoja-Starzewski, M.: Mesoscale bounds in finite elasticity and thermoelasticity of random composites, In: Proceedings of the Royal Society of London A: Mathematical, Physical and Engineering Sciences, vol. 462, pp. 1167–1180. The Royal Society (2006)
20. Ostoja-Starzewski, M.: Material spatial randomness: From statistical to representative volume element. Probab. Eng. Mech. **21**(2), 112–132 (2006)
21. Karim, M., Krabbenhoft, K.: Extraction of effective cement paste diffusivities from X-ray microtomography scans. Transp. Porous Media **84**(2), 371–388 (2010)

22. Ostoja-Starzewski, M., Du, X., Khisaeva, Z., Li, W.: Comparisons of the size of the representative volume element in elastic, plastic, thermoelastic, and permeable random microstructures. Int. J. Multiscale Comput. Eng. 5(2), 73–82 (2007)
23. Du, X., Ostoja-Starzewski, M.: On the size of representative volume element for darcy law in random media. In: Proceedings of the Royal Society of London A: Mathematical, Physical and Engineering Sciences, vol. 462, pp. 2949–2963. The Royal Society (2006)
24. Ostoja-Starzewski, M.: Microstructural Randomness and Scaling in Mechanics of Materials. CRC Press, Boca Raton (2007)
25. Ostoja-Starzewski, M., Ranganathan, S.I.: Scaling and homogenization in spatially random composites. Mathematical Methods and Models in Composites. Imperial College Press, London (2013)
26. Ranganathan, S.I., Ostoja-Starzewski, M.: Scale-dependent homogenization of inelastic random polycrystals. J. Appl. Mech. **75**(5), 051008 (2008)
27. Ostoja-Starzewski, M.: Scale effects in plasticity of random media: status and challenges. Int. J. Plast **21**(6), 1119–1160 (2005)
28. Jiang, M., Ostoja-Starzewski, M., Jasiuk, I.: Scale-dependent bounds on effective elastoplastic response of random composites. J. Mech. Phys. Solids **49**(3), 655–673 (2001)
29. Kanit, T., Forest, S., Galliet, I., Mounoury, V., Jeulin, D.: Determination of the size of the representative volume element for random composites: statistical and numerical approach. Int. J. Solids Struct. **40**(13), 3647–3679 (2003)
30. El Houdaigui, F., Forest, S., Gourgues, A.-F., Jeulin, D.: On the size of the representative volume element for isotropic elastic polycrystalline copper. In: IUTAM Symposium on Mechanical Behavior and Micro-Mechanics of Nanostructured Materials, pp. 171–180. Springer, Berlin (2007)
31. Dalaq, A.S., Ranganathan, S.I., Ostoja-Starzewski, M.: Scaling function in conductivity of planar random checkerboards. Comput. Mater. Sci. **79**, 252–261 (2013)
32. Zhang, J., Ostoja-Starzewski, M.: Frequency-dependent scaling from mesoscale to macroscale in viscoelastic random composites. In: Proceedings of the Royal Society of London A: Mathematical, Physical and Engineering Sciences, vol. 472. The Royal Society (2016)
33. Suquet, P.: Elements of homogenization for inelastic solid mechanics. Homog. Tech. Compos. Media **272**, 193–278 (1987)
34. Hill, R.: The Mathematical Theory of Plasticity. Oxford University Press, Oxford (1950)
35. Quey, R., Dawson, P., Barbe, F.: Large-scale 3D random polycrystals for the finite element method: generation, meshing and remeshing. Comput. Methods Appl. Mech. Eng. **200**(17), 1729–1745 (2011)
36. Ranganathan, S.I., Ostoja-Starzewski, M.: Universal elastic anisotropy index. Phys. Rev. Lett. **101**(5), 055504 (2008)
37. Sab, K.: On the homogenization and the simulation of random materials. Eur. J. Mech. A Solids **11**(5), 585–607 (1992)
38. Huet, C.: Application of variational concepts to size effects in elastic heterogeneous bodies. J. Mech. Phys. Solids **38**(6), 813–841 (1990)
39. Ostoja-Starzewski, M., Kale, S., Karimi, P., Malyarenko, A., Raghavan, B., Ranganathan, S. I., Zhang, J.: Scaling to RVE in Random Media. Adv. Appl. Mech. **49**, 111–211 (2016). doi:10.1016/bs.aams.2016.07.001
40. Hill, R.: The elastic behaviour of a crystalline aggregate. Proc. Phys. Soc. Lond. Sect. A **65**(5), 349–354 (1952)
41. Bhattacharya, K., Suquet, P.: A model problem concerning recoverable strains of shape-memory polycrystals. In: Proceedings of the Royal Society of London A: Mathematical, Physical and Engineering Sciences, vol. 461, pp. 2797–2816. The Royal Society (2005)
42. Berryman, J.G.: Bounds and self-consistent estimates for elastic constants of random polycrystals with hexagonal, trigonal, and tetragonal symmetries. J. Mech. Phys. Solids **53**(10), 2141–2173 (2005)
43. Watt, J.P.: Hashin-Shtrikman bounds on the effective elastic moduli of polycrystals with monoclinic symmetry. J. Appl. Phys. **51**(3), 1520–1524 (1980)
44. Lide, D.R.: Handbook of Chemistry and Physics. CRC Press, Boca Raton (2004)
45. Brown, J.M., Angel, R.J., Ross, N.: Elasticity of plagioclase feldspars. J. Geophys. Res. Solid Earth **121**, 663–675 (2016)
46. Watt, J.P., Peselnick, L.: Clarification of the Hashin-Shtrikman bounds on the effective elastic moduli of polycrystals with hexagonal, trigonal, and tetragonal symmetries. J. Appl. Phys. **51**(3), 1525–1531 (1980)
47. Ledbetter, H., Kim, S.: Monocrystal elastic constants and derived properties of the cubic and the hexagonal elements. Handb. Elast. Prop. Solids Liquids Gases **2**, 97–106 (2001)